Modeling Physiological Resistance in Bacterial Biofilms

N. G. Cogan*
Ricardo Cortez †
Lisa Fauci‡

*Mathematics Department Tulane University New Orleans, LA. 70118 e-mail: cogan@math.tulane.edu FAX: 504 865 5063

†Mathematics Department Tulane University New Orleans, LA. 70118 e-mail: cortez@math.tulane.edu FAX: 504 865 5063

‡Mathematics Department Tulane University New Orleans, LA. 70118 e-mail: ljf@math.tulane.edu FAX: 504 865 5063

Running Title: Modeling Physiological Resistance

Corresponding Author: N. G. Cogan
Mathematics Department
Tulane University
New Orleans, LA. 70118
E-mail: cogan@math.tulane.edu
Phone: 504 862 3439
Fax: 504 865 5063

Submission: Electronic (LaTex)

Abstract

A mathematical model of the action of antimicrobial agents on bacterial biofilms is presented. The model includes the fluid dynamics in and around the biofilm, advective and diffusive transport of two chemical constituents and the mechanism of physiological resistance. Although the mathematical model applies in three-dimensions, we present two-dimensional simulations for arbitrary biofilm domains and various dosing strategies. The model allows the prediction of the spatial evolution of bacterial population and chemical constituents as well as different dosing strategies based on the fluid motion. We find that the interaction between the nutrient and the antimicrobial agent can reproduce survival curves which are comparable to other model predictions as well as experimental results. The model predicts that exposing the biofilm to low concentration doses of antimicrobial agent for longer time is more effective than short time dosing with high antimicrobial agent concentration. The effects of flow reversal and the roughness of the fluid/biofilm are also investigated. We find that reversing the flow increases the effectiveness of dosing. In addition, we show that overall survival decreases with increasing surface roughness.

1 Introduction

Although biofilms are beneficial in some environments such as wastewater management [23], sewage treatment [41] and oilfields [5], much of the focus of research is on deleterious properties of biofilms. In industrial settings these properties include fouling, corrosion and contamination [4]. In medical settings, biofilms are responsible for a wide variety of infections [8]. Recently, it was reported that biofilms may be responsible for up to 65% of all infections [29]. Moreover, bacteria within biofilms are more resistant to antimicrobial agents than are planktonic cells of the same type [2], which poses immediate difficulties in treating biofilm infections.

There are many possible resistance mechanisms that have been introduced in the literature. One mechanism is the inability of the antimicrobial agent to fully penetrate the biofilm region. This is probably not due to reduced diffusion within the biofilm matrix. Rather, it is thought that penetration failure is due to a neutralizing reaction between the antimicrobial agent and some component of the biofilm [9, 12, 35]. Reaction limitation cannot completely explain biofilm resistance, since for antimicrobial agents that are not reactive or for thin biofilms where full penetration can be shown, susceptibility is still reduced substantially [12].

Another possible mechanism is that of physiological resistance. If the bacteria within the biofilm are not respiring, susceptibility to antimicrobial agents is typically decreased [19]. Thus, even if the entire bacterial population is exposed to antimicrobial agent, only the respiring fraction of bacteria are susceptible to killing. This mechanism alone cannot fully explain lowered susceptibility. If the antimicrobial agent can fully penetrate the biofilm and if only the respiring bacteria are susceptible, then as the exposure time is increased, the nutrient would penetrate further into the biofilm region causing bacteria deeper in the biofilm to become susceptible. Hence, exposing the biofilm for longer periods would eventually eradicate the bacteria. This is typically not the case in experimental studies. Instead, biofilms

tend to have a small population of 'persister cells' which are not removed by antimicrobial agent challenge [21], so it is unlikely that physiological resistance operates alone.

It has been proposed [17, 31] that quorum-sensing may be a mechanism by which bacteria can up-regulate resistance mechanisms. It is unclear whether this is done by up-regulation of multi-drug efflux pumps [21] or other mechanism such as expression of a non-growing, peristant phenotype [38]; however, there are indications that interfering with the quorum-sensing communication system may increase bacterial susceptibility [38].

We briefly review two mathematical investigations of resistance mechanisms [32, 33]. In the first of these [33], Sanderson and Stewart investigate the role of dosing protocols for the reactive biocide monochlorimine. The authors assume that there is a fixed amount of material within the biofilm region that neutralizes the biocide. The neutralizing agent is depleted by reaction with the biocide. Mass balance equations are derived for the biocide and the neutralizer. These equations are solved using the numerical simulation package AQUASIM [39] which incorporates bulk flow into and out of a one-dimensional well mixed reactor, transport of dissolved constituents within the biofilm, nutrient consumption, advection of cell mass, cell detachment and bacterial growth. Because the bulk fluid is assumed to be well mixed, the fluid dynamics are not addressed. This model captures gross experimental trends such as rapid disinfection followed by steady regrowth. However, the model predicts that the second dose of monochlorimine is more effective than the initial dose, which is contradicted by experimental data obtained in the same study.

In the second study [32], Roberts and Stewart describe a model of biofilm dynamics used to investigate the role of nutrient limitation on bacterial biofilm susceptibility. The model describes the reaction and diffusion of one limiting substrate and one non-reactive antimicrobial agent within a one-dimensional biofilm. The rate of killing by the agent is assumed to be proportional to the growth rate. Zones of no growth are found within the biofilm due to nutrient uptake and subsequent non-uniform spatial patterns of biofilm microorganism killing. Biofilm susceptibility is shown to depend on the biofilm thickness and on the nutrient source concentration. The model is then extended to include a hypothetical damaged cell state, where cells are nonviable but still consume substrate. This resulted in slowed biofilm killing.

It is important to note that in the above studies, and many other mathematical models of biofilms [11, 39] the external fluid is either stationary or flow effects are incorporated by including the mass-transfer boundary layer as a parameter of the model. One method hat introduces the effects of the fluid dynamics is the one developed by Eberl [13] which separates the bulk fluid region from the heterogeneous biofilm region by a plane located at the maximum height of the biofilm/fluid interface. This substantially simplifies the numerical calculation of the fluid dynamics but it neglects the influence of the biofilm roughness on the flow. In contrast, our goal is to accurately describe the complex interaction between the flowing bulk fluid and the heterogeneous biofilm.

There have been several experimental investigations concerning the effects of flow and the developing biofilm [3, 10, 18, 28, 37, 36]. Flow rate has been shown to have a significant effect on the mass transport of material within the biofilm [3, 10]. This is partly true because the material properties of the developing biofilm depend on the flow environment, but also because the rate of substrate removal depends on the fluid velocity near the biofilm [4, 10].

The fluid dynamics also influence the spatial morphology of the biofilm. Clearly de-

tachment, both large scale sloughing events and slower erosion, is intimately related to the fluid dynamics. Fluid dynamics also have an important effect on the deformation of the biofilm [18, 28, 36, 37]. In general, experimental evidence indicates that neglecting the fluid dynamics may have a significant effect on biofilm processes; therefore, we regard including robust fluid dynamics is of fundamental importance. In fact, the simulations presented in the manuscript show that fluid dynamics does, indeed, influence survival properties of the biofilm.

The present model is the first step in a more comprehensive model that will include detachment and growth processes. Here we are primarily concerned with the effects of the flow on the transport of chemical constituents. Since no a priori assumptions are made on the antimicrobial agent penetration depth or the concentrations in the bulk fluid we may investigate the development of spatial inhomogeneities in bacterial susceptibility, as well as the effects of different dosing protocols, based on manipulating the flow.

If a reaction between the antimicrobial agent and a neutralizing agent within the biofilm is included and external flow is neglected, we obtain quantitative agreement with experimental data [12]. We also find that physiological resistance is capable of capturing the qualitative shape of survival curves as reported in [32]. By direct comparison, we show that plotting survival curves on the scale determined by the product of antimicrobial agent dose concentration and dose duration is not a consistent way to compare dosing protocols. For example, comparing the survival curve for a dosing strategy that calls for continuous dosing of a antimicrobial agent at 10 mg l^{-1} for two hours to a strategy of dosing with concentration 20 mg l^{-1} for one hour is not equivalent on the mixed time scale mg l^{-1}s. The assumption that these survival curves are equivalent has been questioned in the literature and contradicted by experimental results [16]. Our results also contradict this assumption. Motivated by the spatial distribution of the susceptible population, we study the effect of reversing the bulk fluid flow during the antimicrobial agent application. We find that reversing the flow increases the effectiveness of the antimicrobial agent. We also investigate the effect of surface roughness on antimicrobial agent efficacy by simulating several biofilms with varying fluid/biofilm interfaces. We find that survival decreases with increasing surface roughness and that the decrease depends on the flow velocity.

In the following sections we describe the mathematical model and the numerical methods used to solve the coupled fluid, biofilm, antimicrobial agent, nutrient system of partial differential equations. We then detail several two-dimensional numerical experiments and results.

2 Model Equations

We describe the governing equations for a two-dimensional biofilm in the presence of a single nutrient, oxygen, and a single antimicrobial agent. The biofilm is assumed to be attached to one of the walls of a channel and we include the flow of a fluid in the portion of the channel that is exterior to the biofilm (refer to Figure 1). The fluid flow transports the nutrient and the agents. The following two sections describe the geometry and the equations of the model.

2.1 The Fluid Flow

We consider a physical domain consisting of a channel of width mL and length L. In the channel we assume that there is a steady, creeping flow and that there is a biofilm attached to one of the channel walls and partially obstructing the flow. The biofilm region is bounded by a fluid/biofilm interface, denoted Γ, and a portion of the bottom wall along the x-axis (see Figure 1). Throughout this investigation we assume that the shape of the biofilm does not change in time. In other words, we restrict the study to phenomena that occur while the biofilm morphology is constant. In our study, this assumption is reasonable because the time scale of disinfection is sufficiently shorter than that of biofilm growth. Future extensions of the model presented here will include biofilm morphology changes due to growth and fluid/structure interactions as well as the process of detachment. All of these are important and are currently under investigation [18, 28].

Since the length scale is small and the fluid velocities are low (see Table II) the Reynolds number is on the order of 10^{-4}. Therefore, we assume that the fluid velocity, $\vec{U}$, is governed by the incompressible Stokes equations

$$\mu \Delta \vec{U} = \nabla p - \vec{F} \tag{1}$$

$$\nabla \cdot \vec{U} = 0, \tag{2}$$

where μ is the fluid viscosity and p is the pressure. In all of our simulations, the fluid velocity $\vec{U}$ will be the superposition of a parabolic flow from left to right, which is the flow that develops in a channel without obstructions, and a disturbance flow due to the presence of the biofilm. The forces $\vec{F}$, applied to the fluid/biofilm interface Γ and to the channel walls, are computed so that the resultant velocity $\vec{U}$ is zero along those boundaries. It turns out that since the fluid velocity is zero along all boundaries enclosing the biofilm, the flow is negligible within the entire biofilm region [7].

Since the geometry of the channel and the biofilm does not change in time, the fluid flow satisfying all appropriate boundary conditions on the fluid/biofilm interface and on the channel walls can be computed only once and it remains unchanged for the rest of the simulation. For this reason, we compute the fluid flow first and then use this flow to compute the dynamics of the chemical constituents.

2.2 The Dynamics of the Constituents

Nutrient, $S(\vec{x}, t)$, and antimicrobial agent, $A(\vec{x}, t)$, are introduced into the system at the left end of the domain. Both are advected by the fluid flow and diffuse within the fluid and the biofilm. Since the flow is zero in the biofilm region, the nutrient and the antimicrobial agent penetrate the biofilm only through the process of diffusion. The diffusion coefficients of nutrient and antimicrobial agent, $D_s(\vec{x})$ and $D_a(\vec{x})$, are assumed to be smaller in the biofilm region than in the flow region. The reduction factors are denoted r_s and r_a, respectively. The consumption of nutrient by the bacteria is modeled by Monod kinetics, where μ_s, Y_s and K_s denote the maximum specific growth rate, yield coefficient and Monod coefficient, respectively. These assumptions yield the following equations:

$$\frac{\partial S(\vec{x}, t)}{\partial t} + \vec{U}(\vec{x}, t) \cdot \nabla S(\vec{x}, t) = \nabla \cdot (D_s \nabla S(\vec{x}, t)) - \mu_s \frac{S}{K_s + S} B(\vec{x}, t) \tag{3}$$

$$\frac{\partial A(\vec{x},t)}{\partial t} + \vec{U}(\vec{x},t)\cdot\nabla A(\vec{x},t) = \nabla\cdot(D_a\nabla A(\vec{x},t)) - H_a(A,N). \quad (4)$$

The population of viable bacteria is denoted $B(\vec{x},t)$. The function H_a denotes the reaction between the antimicrobial agent and the concentration of neutralizing agent, denoted N, within the biofilm. For the simulations below, H_a is either zero or, if $H_a \neq 0$, we assume that the neutralizing agent is consumed by the reaction at a rate proportional to the product of A and N, in particular we set $H_a = -k_r AN$. Note that H_a depends only on the neutralizer and antimicrobial concentrations and is independent of B. The dynamics of the neutralizer are,

$$\frac{\partial N(\vec{x},t)}{\partial t} = -k_r Y_n AN, \quad (5)$$

where Y_n denotes the neutralizer/antimicrobial agent yield coefficient.

Finally, the effect of the antimicrobial agent on the bacteria is included in the following equation for the population of bacteria within the biofilm region,

$$\frac{\partial B}{\partial t} = -p_1(A,S)B, \quad (6)$$

where B is zero outside the biofilm region and $p_1(A,S)$ denotes the disinfection rate.

The description of the disinfection rate, $p_1(A,S)$, differs for various antimicrobial agents and disinfection models. There are many factors that affect this term, including the nature of persister cells and the process of physiological resistance. We assume that bacteria are susceptible to the agent at a rate proportional to the product of the agent concentration and the bacterial growth rate. Because the growth rate depends on the nutrient concentration, bacteria that are in nutrient-limited zones (i.e. deep within the biofilm) are not susceptible. Tacit in this model is that the maximum specific growth rate is constant. In [38], it is suggested that variations in maximum specific growth rate may also affect the spatial variation of bacterial susceptibility. For the simulations presented below, we set $p_1 = \kappa Y \mu_s A \frac{S}{K_s+S}$, where Y is the yield coefficient and κ is a constant of proportionality.

For computational purposes, the equations are nondimensionalized introducing the dimensionless variables $x^* = \frac{x}{L}$, $t^* = \frac{t}{T}$, $\vec{U}^* = \frac{\vec{U}T}{L}$, $P^* = \frac{P\mu}{T}$, $A^* = \frac{A}{a}$, $S^* = \frac{S}{K_s}$ $N^* = \frac{N}{n}$ and $B^* = \frac{B}{b}$ into the system of Equations (1) - (6). The parameters T, a, n and b are typical time and concentration scales. The nondimensional equations are

$$\Delta\vec{U}^* = \nabla P^* - F^* \quad (7)$$

$$\nabla\cdot\vec{U}^* = 0 \quad (8)$$

$$\frac{\partial S^*}{\partial t^*} + \vec{U}^*\cdot\nabla S^* = -\mu_s^*\frac{S^*}{1+S^*}B^* + \nabla\cdot(D_s^*\nabla S^*) \quad (9)$$

$$\frac{\partial A^*}{\partial t^*} + \vec{U}^*\cdot\nabla A^* = \nabla\cdot(D_a^*\nabla A^*) - k_r n A^* N^* \quad (10)$$

$$\frac{\partial N^*}{\partial t} = -k_r^* A^* N^* \quad (11)$$

$$\frac{\partial B^*}{\partial t^*} = -p_1^*(aA^*, k_s S^*)B^*, \quad (12)$$

where $\mu_s^* = \frac{\mu_s T}{K_s} b$, $D_s^* = \frac{TD_s}{L^2}$, $D_a^* = \frac{TD_a}{L^2}$, $k_r^* = ak_r Y_n$ and $p_1^* = Tp_1$. The nondimensional domain is $(0,1) \times (0,m)$. The boundary conditions associated with the nondimensional system above are $\vec{U}^* = 0$ on the fluid/biofilm interface, Γ, and the channel walls, $y = 0$, $y = m$. As discussed earlier, the velocity $\vec{U}^*$ is the superposition of a parabolic flow whose maximum speed is denoted U_{max} and a disturbance flow due to the presence of the biofilm. The chemical constituents satisfy $\frac{\partial A^*}{\partial y} = \frac{\partial S^*}{\partial y} = 0$ at $y = 0, y = m$. For the simulations shown below, the concentration of antimicrobial agent and nutrient are the constants C_a and C_s at the upstream end of the domain.

3 Numerical Methods

The numerical solution of the coupled equations of the fluid/biofilm/chemical system described above presents a number of challenges. Foremost is the irregularity of the interface that separates the fluid region from the biofilm region. The gel-like structure of biofilm indicates that this interface is typically diffuse in biofilm settings [40]. The density of the biofilm changes rapidly and diffusion coefficients of dissolved or suspended constituents within the biofilm depend on the density of the biofilm [34]. Hence, this interface Γ supports a transition region across which the diffusion coefficients of the chemical constituents, while continuous, vary rapidly. The width of this transition region is a physical parameter that is chosen to reflect the structure of the biofilm, rather than a numerical parameter that tends to zero.

For the chemical constituents, we adopt a computational framework that discretizes the rectangular region of the channel (including the biofilm) using a regular, finite difference grid. The biofilm interface is represented by a discrete collection of points that do not coincide with grid points. This discretized interface is used to assign appropriate values of diffusion coefficients to grid points that fall within the transition region. This will be described below.

For the fluid flow computation, we use the interface points together with the discrete points along the channel walls to compute the steady fluid velocity field using the method of regularized Stokeslets. This grid-free method exploits the linear relationship between the fluid velocity at the boundary points and the forces applied at those same points. The disturbance flow due to the biofilm presence must be such that it cancels the background parabolic flow at the fluid/biofilm interface Γ. This is done by imposing the appropriate velocity conditions at all the boundary points and solving a linear system for the forces at those points. Now the superposition of the parabolic flow and the disturbance flow will produce the correct fluid velocity. Once the forces are computed, the fluid velocity at any point in the domain can be written as a linear combination of flow contributions from each of the forces plus the parabolic flow. These contributions are exact solutions of the Stokes equations due to the presence of regularized forces. In particular, we can evaluate the fluid velocity field at all lattice points on the finite difference grid to be used in the evolution of the chemical constituents. Because both the fluid flow and the geometry of the interface do not change in time, we need to compute this velocity field only once at the beginning of the simulation.

The solution of the fluid equations, and the solution of the evolution equations of chemical transport do not treat the interface as a sharp interface, but allow for a smoothed-out region where fluid forces are applied and where diffusion coefficients smoothly vary. Estimates of

the thickness of this 'mushy' zone depend on the age of the biofilm, bacterial growth rates and limiting nutrients [4]; however, measurements of biofilm densities [42, 4] indicate that the density typically increases with the depth within the biofilm. For example, Characklis [4], reports that the density of a 730 μm thick biofilm varies from 37 kg m^{-3} in the top 400 μm to 102 kg m^{-3} in the bottom 130 μm. Zhang and Bishop [42] report a density of 15 mg cm^{-3} in the surface layers and 105 mg cm^{-3} in the bottom layers. We assume that the transition layer is approximately 200 μm thick for the simulations below.

3.1 Fluid Dynamics

Solving Equations (1) and (2) requires enforcing boundary conditions at the channel walls and the fluid/biofilm interface, which is irregular. The solution is obtained using the method of regularized Stokeslets [6] described in more detail below. We first specify a parabolic background flow, with maximum flow rate U_{max}, in the absence of the interface points. The basic idea of the method is to apply boundary forces, $\vec{F}$, so that the superposition of the parabolic background flow and the disturbance flow due to the forces satisfies all the boundary conditions simultaneously.

A fundamental solution of the incompressible Stokes equations is called a Stokeslet, and it represents the velocity due to a concentrated force acting on the fluid at a single point in an infinite domain of fluid [22]. The Stokeslet for a single force applied at the origin in two-dimensions is

$$\vec{U}_s(\vec{x}) \;=\; -\frac{\vec{f}_0}{4\pi\mu}\ln(r) + (\vec{f}_0\cdot\vec{x})\frac{\vec{x}}{4\pi\mu r^2},$$

where $\vec{f}_0$ is the magnitude of the force and $r = |\vec{x}|$.

Because this expression is singular at the origin (the point where the force is applied), it is difficult to evaluate numerically. Cortez considers the smoothed case where the concentrated force is applied not at a single point, but over a small ball of radius δ centered at the origin [6]. Smoothing the forces results in an exact solution to Equations (1) and (2) with the distributed force given by

$$\vec{F}(\vec{x}) \;=\; \vec{f}_0\phi_\delta(\vec{x}),$$

for a given cutoff function ϕ_δ. These functions approximate the Dirac δ-function and generally have the shape of a tight Gaussian with total integral equal to one. Once ϕ_δ is specified, we can solve Equations (1) and (2) analytically. For example, the cutoff function

$$\phi_\delta(\vec{x}) = \frac{3\delta^3}{2\pi(r+\delta^2)^{5/2}},$$

yields the exact velocity

$$\begin{aligned}\vec{U}_\delta \;=\; & -\frac{\vec{f}_0}{4\pi\mu}\left(\ln\left(\sqrt{r^2+\delta^2}+\delta\right) - \frac{\delta\left(\sqrt{r^2+\delta^2}+2\delta\right)}{\left(\sqrt{r^2+\delta^2}+\delta\right)\sqrt{r^2+\delta^2}}\right) \\ & +\frac{1}{4\pi\mu}\left(\vec{f}_0\cdot\vec{x}\right)\vec{x}\left(\frac{\sqrt{r^2+\delta^2}+2\delta}{\left(\sqrt{r^2+\delta^2}+\delta\right)^2\sqrt{r^2+\delta^2}}\right). \qquad (13)\end{aligned}$$

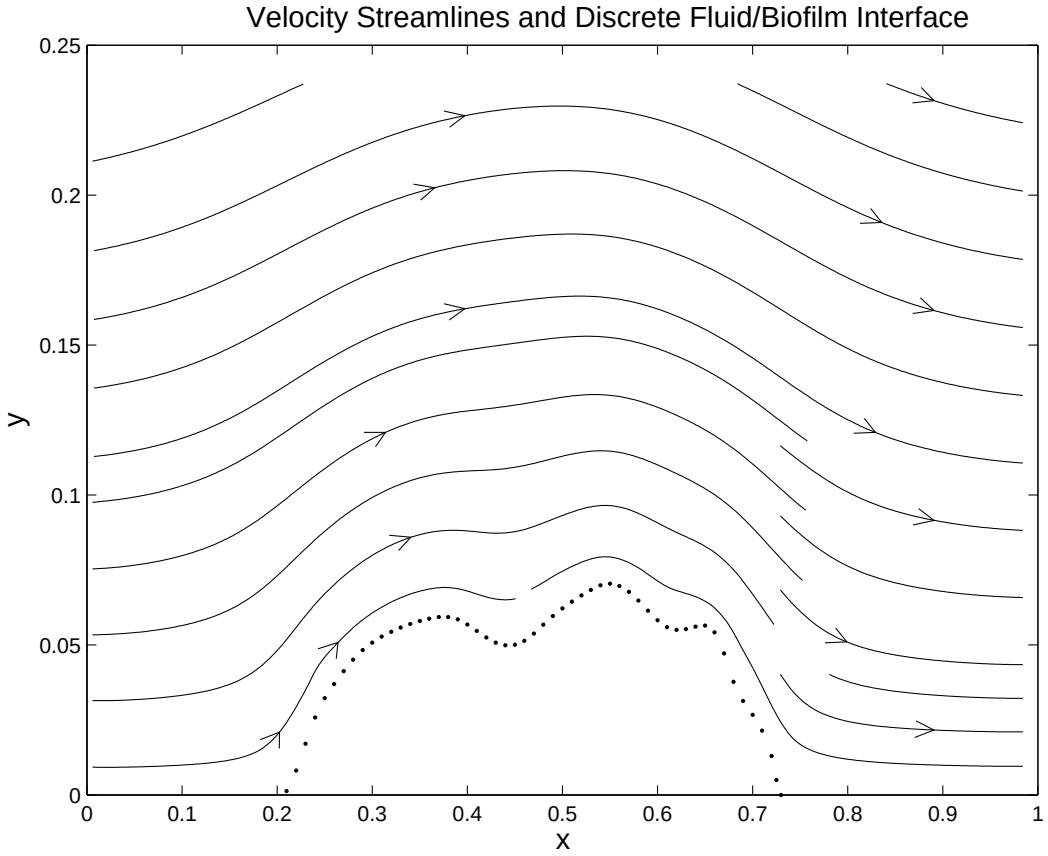

Figure 1: Example of the discretized fluid/biofilm interface with the calculated velocity streamlines. Note that there is no advection within the biofilm region.

In the limit $\delta \to 0$ we obtain the classical formulas; however, $\vec{U}_\delta$ has the advantage of not being singular.

Since the Stokes equations are linear, one may represent the final flow as a direct summation of contributions from finitely many discrete forces. The forces we are concerned with are those due to the presence of the biofilm. By discretizing the boundaries (the fluid/biofilm interface and the channel walls), we obtain a finite number of points at which there are applied forces. The same points are used to enforce the no-flow condition. That is, the forces to be computed must cancel the parabolic flow so that after the superposition of the disturbance flow due to forces and the parabolic flow, the velocity is zero at the boundary points along the interface Γ and the channel walls. The forces are computed by setting up a linear system based on Equation (13) and inverting the resulting matrix. The velocity field used in our simulations is the sum of the parabolic flow plus expressions like that in Equation (13), one for each force applied at the boundary points. Streamlines for the velocity around an example region are shown in Figure 1.

The method of regularized Stokeslets is related to boundary integral methods, but has the advantage that forces may be applied at any discrete collection of points. It should be emphasized, that this method is 'grid-free'. That is, $\vec{U}(\vec{x})$ is obtained as a sum of analytic functions. This summation can then be evaluated on our finite-difference grid.

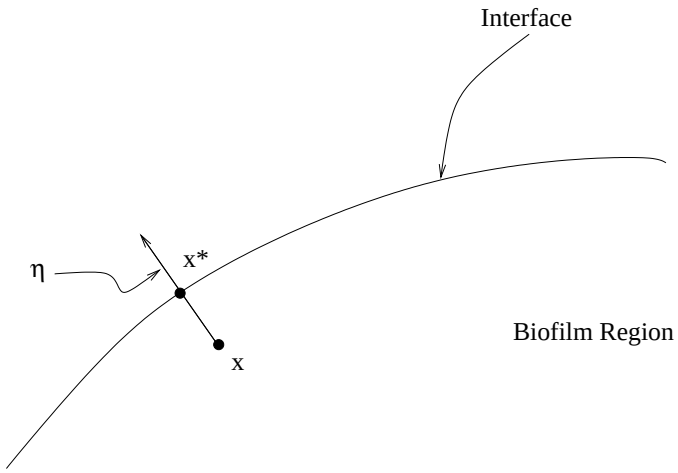

Figure 2: Sketch of the fluid/biofilm interface. The point on the interface nearest to x is x^* and lies in the normal direction.

3.2 Chemical Constituents

Once the steady-state velocity is obtained, Equations (9) - (12) determine the time evolution of the nutrient and biocide concentrations and the bacterial density. The interface between the bulk fluid and the biofilm region is irregular and not aligned with the grid. At the interface, the coefficients experience significant variation.

To incorporate this feature into our model we assume that there is a transition layer of fixed spatial extent where the diffusion coefficients of the constituent particles vary from D_* in the fluid region to r_*D_* in the biofilm. The signed distance from a given point $\vec{x}$ to the interface is $\xi = (\vec{x}^* - \vec{x}) \cdot \vec{\eta}$, where $\vec{x}^*$ is the point on the interface nearest $\vec{x}$ and $\vec{\eta}$ is the outward unit normal at $\vec{x}^*$ (see Figure 2). The diffusion coefficient is given by

$$\hat{D}_*(\vec{x}) = \begin{cases} D_*, & \text{for } \xi \le -\delta \\ D_* + (r_*D_* - D_*)H_\delta(\xi), & \text{for } |\xi| \le \delta \\ r_*D_*, & \text{for } \xi \ge \delta. \end{cases}$$

Where the transition function, $H_\delta(\xi)$, is a smooth approximation of a Heaviside function that is one in the biofilm region and zero in the bulk fluid. The width of the transition layer between D_* and r_*D_* is denoted δ and is specified independently of the discretization. Figure 3 shows contours of the smoothed diffusion coefficient for the region shown in Figure 1.

Various transition functions can be designed but in our calculations we use the transition function

$$H_\delta(\xi) = \begin{cases} 0, & \text{for } \frac{\xi}{\delta} \le -1 \\ \frac{1}{2}(1 + \frac{\xi}{\delta})^2, & \text{for } -1 \le \frac{\xi}{\delta} \le 0, \\ 1 - \frac{1}{2}(1 - \frac{\xi}{\delta})^2, & \text{for } 0 \le \frac{\xi}{\delta} \le 1 \\ 1 & \text{otherwise.} \end{cases}$$

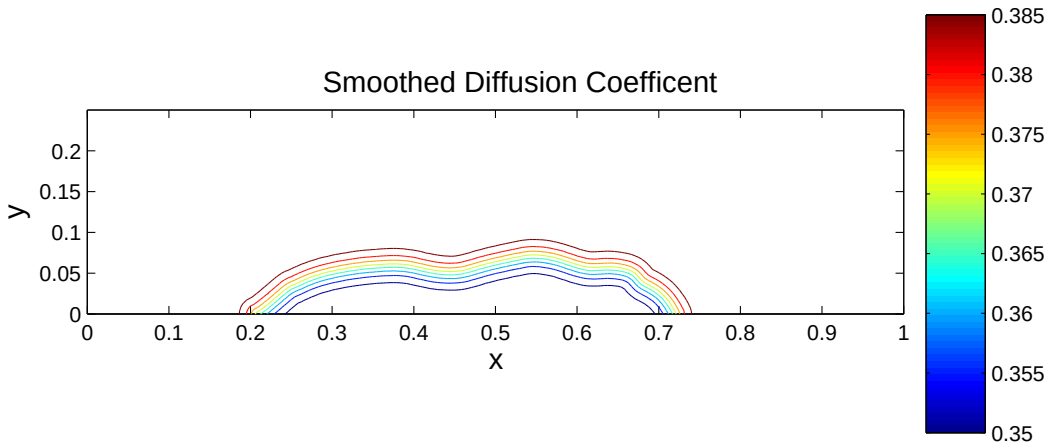

Figure 3: Contours of the diffusion coefficient (m^2h^{-1}) with diffuse boundary. Notice that the transition region is of uniform width which is independent of the mesh spacing.

Once the diffusion coefficients are determined, we use a standard staggered grid approximation of $\nabla \cdot (D(\vec{x})\nabla c)$ [15]. This, in conjunction with a forward-time-center-space discretization of the parabolic operator $\frac{\partial c}{\partial t} - \nabla \cdot (D(\vec{x})\nabla c)$ [15] and upwinding for the advective terms, yields an implicit method which is solved using ADI [30]. The method described above has the advantage of specifying the extent of the diffuse interface independent of the grid.

3.3 Test problem

To validate the method described above, we consider the steady-state diffusion of a chemical where the diffusion coefficient is spatially dependent. We use the test problem presented in [1] for which the analytic solution is available for comparison. The computational domain, $(-1,1) \times (-1,1)$, is separated into two regions, one inside the circle of radius $1/2$ and the other outside the circle. The diffusion coefficient is specified in each region. Mathematically, we solve the equation

$$\nabla \cdot (\beta_\delta(x,y)\nabla u(x,y)) = f(x,y) \tag{14}$$

where the diffusion coefficient is given by

$$\beta_\delta(x,y) = \begin{cases} b, & \text{outside the circle,} \\ b + (x^2+y^2+1-b)H_\delta(\xi), & \text{in the transition,} \\ x^2+y^2+1, & \text{inside the circle.} \end{cases}$$

The forcing function is $f(x,y) = 8(x^2+y^2)+4$ and b is a constant. The problem is specified by imposing Dirichlet boundary conditions on the computational domain.

For each fixed value of δ, we solve Equation (14) by applying the method described above. If the mesh size used for the finite difference discretization of the derivatives is decreased while keeping δ fixed, we find that the method converges quadratically to the solution of the smoothed problem. In Table I, we compare solutions for $\delta = 0.08$ and decreasing mesh spacing which is chosen small enough to have several mesh points in the transition region.

A weak solution to the problem corresponds to the case of discontinuous coefficient $\beta_0(x, y)$ (or $\delta \to 0$). The solution is:

$$u(x,y) = \begin{cases} x^2 + y^2, & \text{for } x^2 + y^2 < \frac{1}{4}, \\ (1 - \frac{1}{8b} - \frac{1}{b})/4 + (\frac{(x^2+y^2)^2}{2} + x^2 + y^2)/b, & \text{for } x^2 + y^2 \geq \frac{1}{4}. \end{cases}$$

The solution is continuous but has a jump in the normal derivative along the circle given by

$$\left[\frac{\partial u}{\partial \eta}\right] = \frac{5}{4b} - 1.$$

Our numerical method approximates this solution. In fact, one can see that for a fixed mesh size, decreasing the value of the smoothing parameter δ results in linear convergence to the weak solution of the problem (Figure 4). By reducing the mesh size and δ simultaneously, our numerical method converges to the solution of the problem with discontinuous coefficients.

3.4 Numerical Results

In the following sections we describe results from our simulations. By integrating the bacterial population in space, we can compute the number of surviving bacteria as a function of time (i.e. survival curve). The survival curves are plotted on a logarithmic scale, where the vertical axis is the logarithm of the ratio between the total population of the remaining viable bacteria to the initial population. We assume that oxygen is the limiting substrate. The parameters used in these simulations are given in Table II. The general trend of the survival curves are consistent with the data in [12], with a relatively slow initial decrease in the surviving population, followed by a sharper decrease, although the time scales depend on the flow rate.

We first demonstrate that, in the absence of flow, but with antimicrobial agent neutralization, we can quantitatively fit experimental data [12]. Then, by incorporating the fluid dynamics into the model, and assuming that the antimicrobial agent is non-reactive, we obtain survival curves that are in qualitative agreement with one-dimensional models [32]. We then show that under the assumptions described above, dosing at low antimicrobial agent concentration for longer durations is more effective than higher dose concentration for shorter periods.

These three simulations are designed to validate the current model; however, one of the strengths of the present study is that it tracks spatial evolution of chemical concentrations

h	$\|\|u_h - u_{2h}\|\|_\infty$
0.01	9.307×10^{-4}
0.005	3.065×10^{-4}
0.0025	8.261×10^{-5}

Table I: Comparison between subsequent mesh refinements. The finite difference stencils and numerical convergence are approximately second order. The support of the transition function is $\delta = 0.08$ and $b = 0.5$.

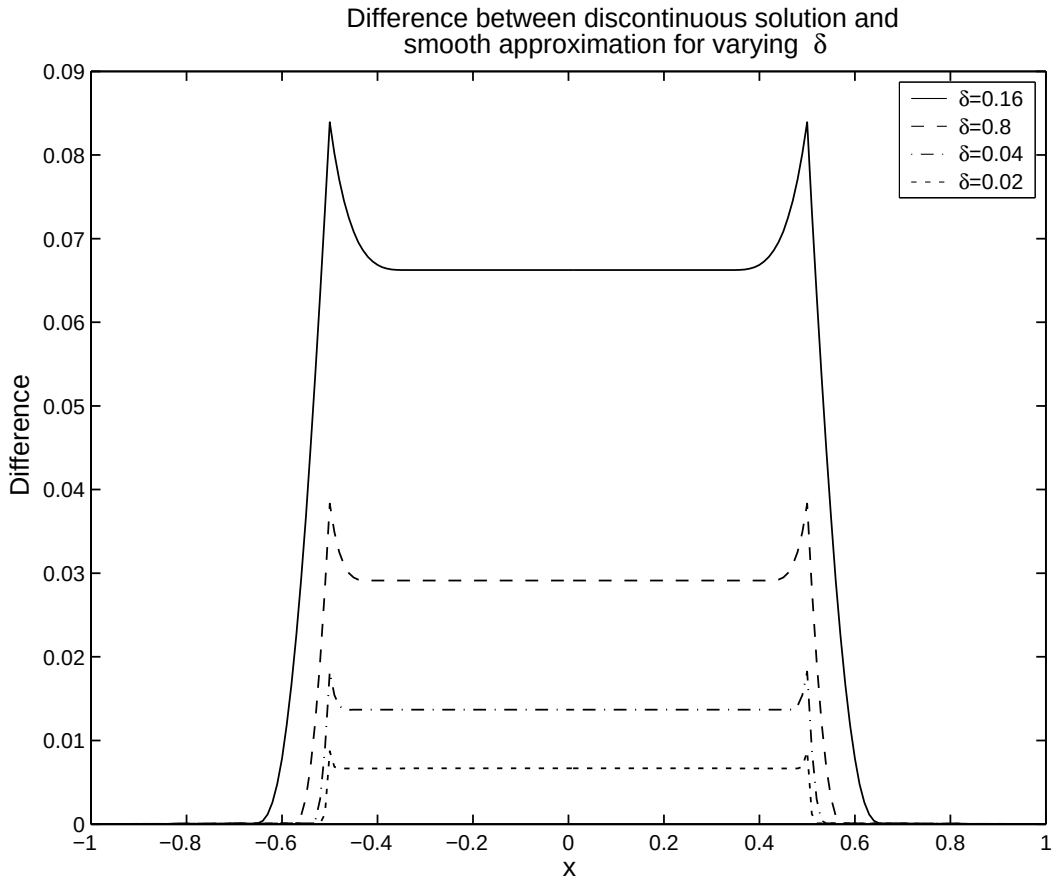

Figure 4: Comparison of errors between the weak solution and the numerical approximation for decreasing δ. The plots show the difference between the true and approximate solution for fixed $y = 0$. The error is localized near the interface $x = \pm\frac{1}{2}$. Here $b = 0.5$ and $h = 0.005$.

Parameter	Symbol	Units	Value	Source
Maximum Specific Growth Rate	μ_s	h^{-1}	0.417	[32]
Yield Coefficient	Y_b		0.8	[32]
Monod Coefficient	K_s	mg l^{-1}	0.1	[32]
Antimicrobial Agent Influent Concentration	C_a	mg l^{-1}	5 - 20	[32]
Nutrient Influent Concentration	C_s	mg l^{-1}	10	[32]
Nutrient Diffusion Coefficient	D_s	m^2h^{-1}	9.67×10^{-6}	[32]
Antimicrobial Agent Diffusion Coefficient	D_s	m^2h^{-1}	1.80×10^{-6}	[32]
Biofilm/Bulk Diffusivity Reduction	r_*		0.9	[33]
Length Scale	L	m	10^{-2}	Assumed
Max. Flow Rate	U_{max}	m h^{-1}	0-3.4	Assumed
Neutralizer Reaction Rate Coefficient	k_r	m^3 g^{-1} h^{-1}	10	[33]
Neutralizer Reaction Yield Coefficient	Y_n	g g^{-1}	3	[33]
Disinfection Rate Coefficient:	κ			
non-reactive antimicrobial agent			0.044	Assumed
reactive antimicrobial agent			0.4	Assumed

Table II: Parameters used in the simulations

and bacterial population. We can use the spatial variability to help determine effectiveness of treatment as well as the distribution of affected cells.

The biofilm domains were arbitrarily initialized on a domain on the scale of two centimeters. The maximum thickness of the biofilm domains is approximately 500 μm, and the leading edge of the biofilm is located between 0.2 and 0.4 centimeters from the influent end of the channel depending on the simulation.

3.5 Simulation 1: No-flow, reactive antimicrobial agent

Although including fluid dynamics is an important part of the current investigation, the model can also be used to simulate no-flow experiments. In [12], Dodds and Stewart incorporated *Pseudomonas aeruginosa* bacteria into alginate gel beads, forming artificial biofilms. These were incubated in a nutrient broth overnight and then suspended in a hypochlorite solution. Multiple gel beads were removed at regular intervals and dissolved. The surviving bacteria were enumerated from the resulting cell suspensions. Hypochlorite is known to be reactive [33]; therefore, we include reaction with a neutralizing agent within the biofilm. The neutralizing agent is assumed to be uniformly distributed within the biofilm and the initial concentration is set to be 4% of the biomass concentration. The neutralizer reacts with the antimicrobial agent, removing the neutralizer and the antimicrobial agent. Because the antimicrobial agent/neutralizer reaction consumes the neutralizing agent, the antimicrobial agent will eventually fully penetrate the biofilm region. For this simulation we solve Equations (7)- (12) with $\vec{U}$ identically zero. The biofilm domain is the same as in Figure (1). The concentrations of antimicrobial agent and nutrient are fixed at their source values outside the biofilm region. The active bacteria are assumed to be uniformly distributed throughout the

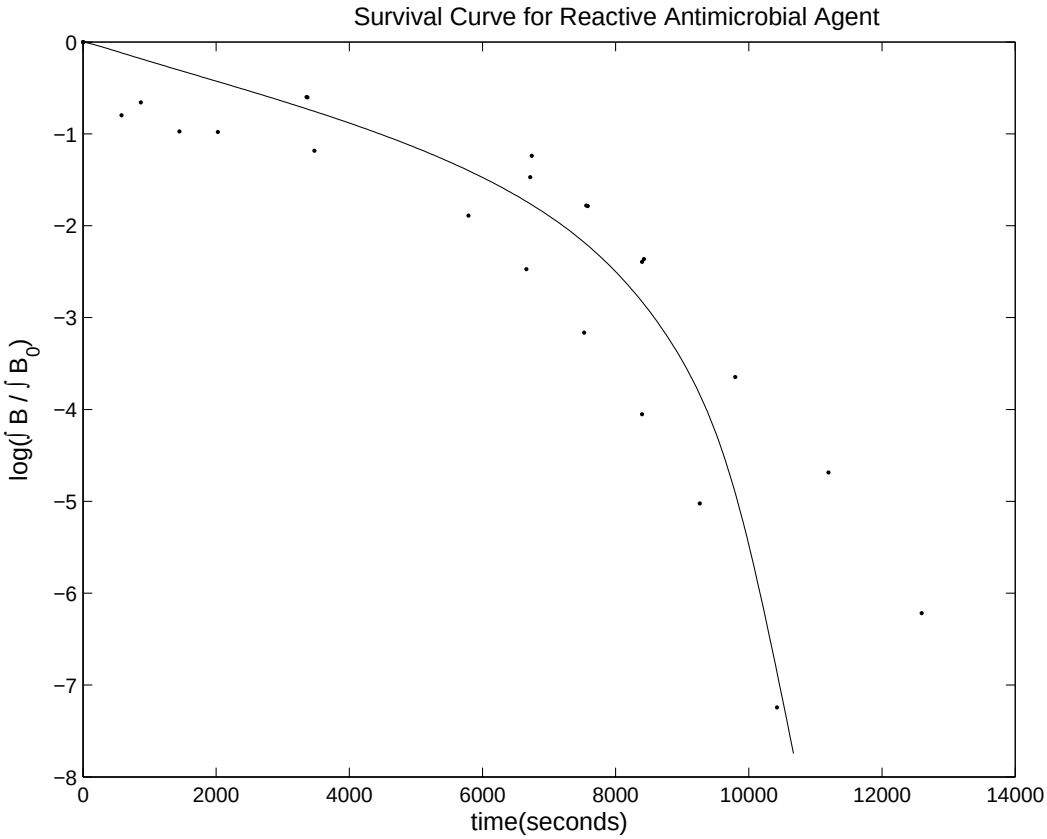

Figure 5: Survival curve for dosing at $C_s = 10\text{mgl}^{-1}$. In this simulation there is no flow and the antimicrobial agent is assumed to react with a neutralizing component of the biofilm. This is consistent with the data collected in [33]. There were multiple samples taken and all the collected data are shown.

biofilm region initially. We then simulate the dynamics for the antimicrobial agent, nutrient, bacteria and neutralizer. Figure 5 shows the survival curve obtained after continuous dosing for 4 hours along with data from [33].

3.6 Simulations 2 and 3: Continuous flow, non-reactive antimicrobial agent

By physiological resistance, we mean that only the bacteria that are respiring are susceptible to antimicrobial agent. It is well known that there are nutrient-depleted zones within the biofilm and that bacteria occupying these zones are typically less susceptible to the antimicrobial agent than actively respiring bacteria [31]. In the following sections we simulate the effect of continuous dosing of a non-reactive antimicrobial agent on a biofilm with a single limiting nutrient.

In this simulation, a background flow from left to right moves in the channel around the biofilm. Initially, the bacteria are uniformly distributed throughout the biofilm region, shown in Figure (1), and the antimicrobial agent and nutrient concentrations are zero within the

computational domain, except at the entrance to the channel where they are fixed at their source concentrations. Snapshots of the concentration of antimicrobial agent, nutrient and active bacteria for various times are shown in Figure 6. The nutrient and antimicrobial agent are advected by the fluid outside the biofilm region. Within the biofilm there is negligible flow, so diffusive transport dominates. However, because the bacteria are consuming oxygen, there are zones within the biofilm where the bacteria are in an anaerobic environment. We note that downstream regions of the biofilm have less exposure to nutrient because of consumption by bacteria upstream, so the anaerobic region is located preferentially towards the downstream end of the biofilm. Since the antimicrobial agent is assumed to be non-reactive in this simulation, we fix N to be zero. We see full antimicrobial agent penetration of the biofilm region. Bacteria in regions where there is both nutrient and antimicrobial agent (near the interface) are killed.

The survival curves for several different flow rates are shown in Figure 7. We see that the 'knee' of the curve occurs earlier for the higher flow rate. Moreover, the overall effectiveness of the treatment is improved. These results imply that more bacteria are exposed to the combination of antimicrobial agent and nutrient when the flow is higher. The qualitative survival curves are similar to those found in [32]. Increasing the flow rate has the effect of decreasing the mass transfer boundary layer, which increases the susceptibility. This is also in qualitative agreement with results from [32].

We next consider whether increasing the concentration of antimicrobial agent and decreasing the length of the dosing application yields equivalent survival curves. In particular, we compare three protocols: dose concentrations of 5 mg l^{-1}, 10 mg l^{-1} and 20 mg l^{-1} for duration 5 hours, 2.5 hours and 1.25 hours, respectively. The survival curves are plotted on the scale of mg l^{-1}s (Figure 8). On this mixed time scale, the domains of the survival curves for the three simulations are the same. We find that the final survival fraction for longer exposure is two orders of magnitude less than that of the shortest dose duration, indicating a more effective treatment.

3.7 Simulation 4: Flow reversal, non-reactive antimicrobial agent

Noting that the upstream region of the biofilm has higher nutrient concentration (last row of Figure 6), and is therefore more susceptible to antimicrobial agent, we investigated the survival curve that is obtained when the flow and dose location are reversed during the simulation. Initially, the flow is from left to right. The initial concentrations of the antimicrobial agent and nutrient are zero except at the influent end of the channel. Midway in the simulation, the flow and dose location are reversed. The flow is then continuous from right to left and the concentrations of antimicrobial agent and nutrient are fixed at the right-hand-side of the channel. Although there are many situations where this is not a viable procedure (for example in biofilm infected artificial joints), there are many industrial settings, such as waste water treatment, where flow reversal is feasible. Intuitively, we expect that reversing the flow will increase the susceptibility of the bacteria by providing the downstream biofilm with nutrient during the dose application. We simulate a dosing experiment in which the flow direction and dose location are reversed after 90 minutes. Because bacteria downstream of the source are exposed to less nutrient, they are less susceptible to the antimicrobial agent. When the flow is reversed, these bacteria become more susceptible, increasing the effective-

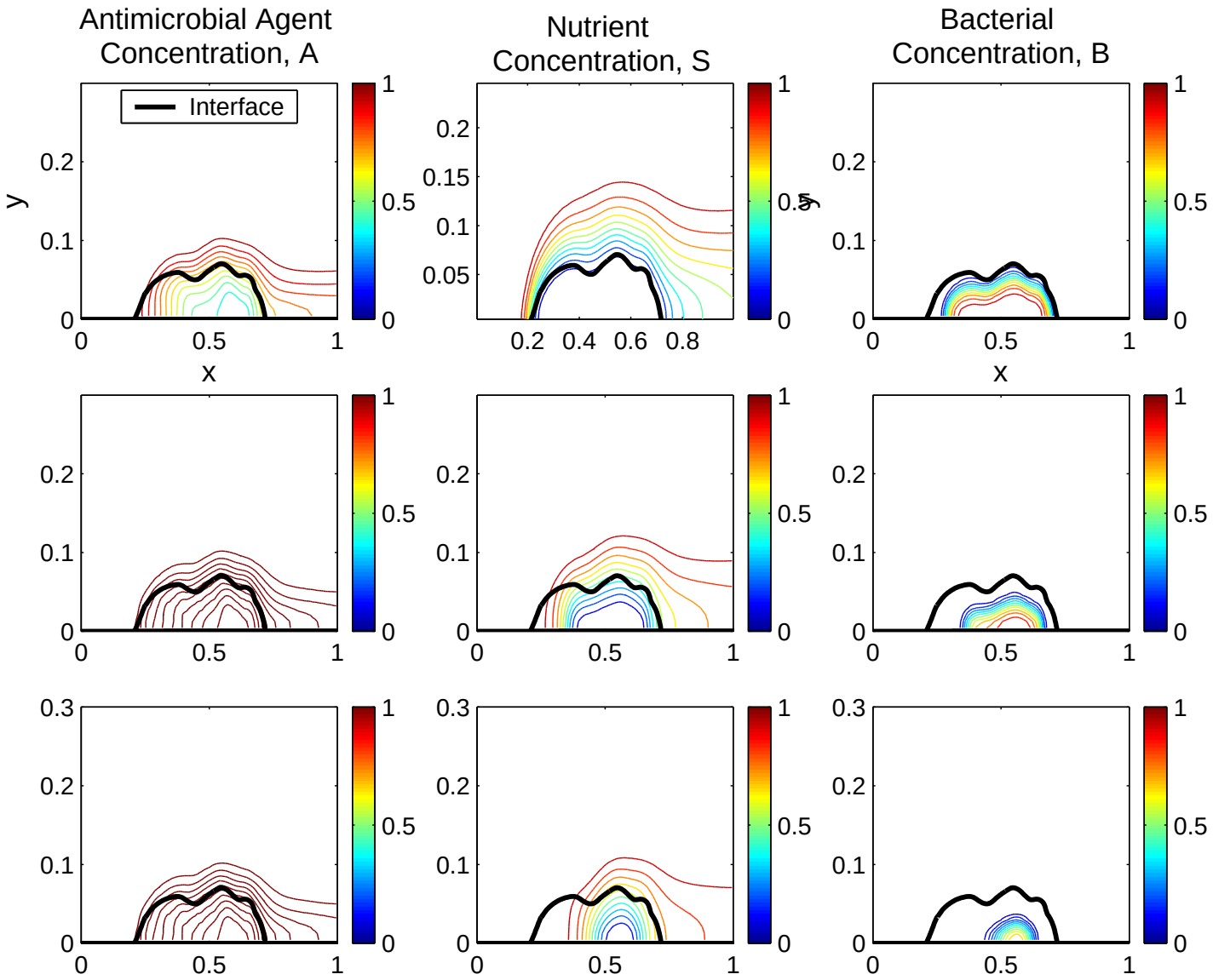

Figure 6: Profiles of antimicrobial agent, nutrient and bacterial concentrations at t=60 minutes (first row), t=120 minutes (second row) and 168 minutes (last row). Note that the antimicrobial agent concentration has equilibrated to the source concentration within two hours (last two rows of the first column) as indicated by the value of the contours. The maximum flow rate for the parabolic background flow is $U_{max} = 0.0334$ m h^{-1}.

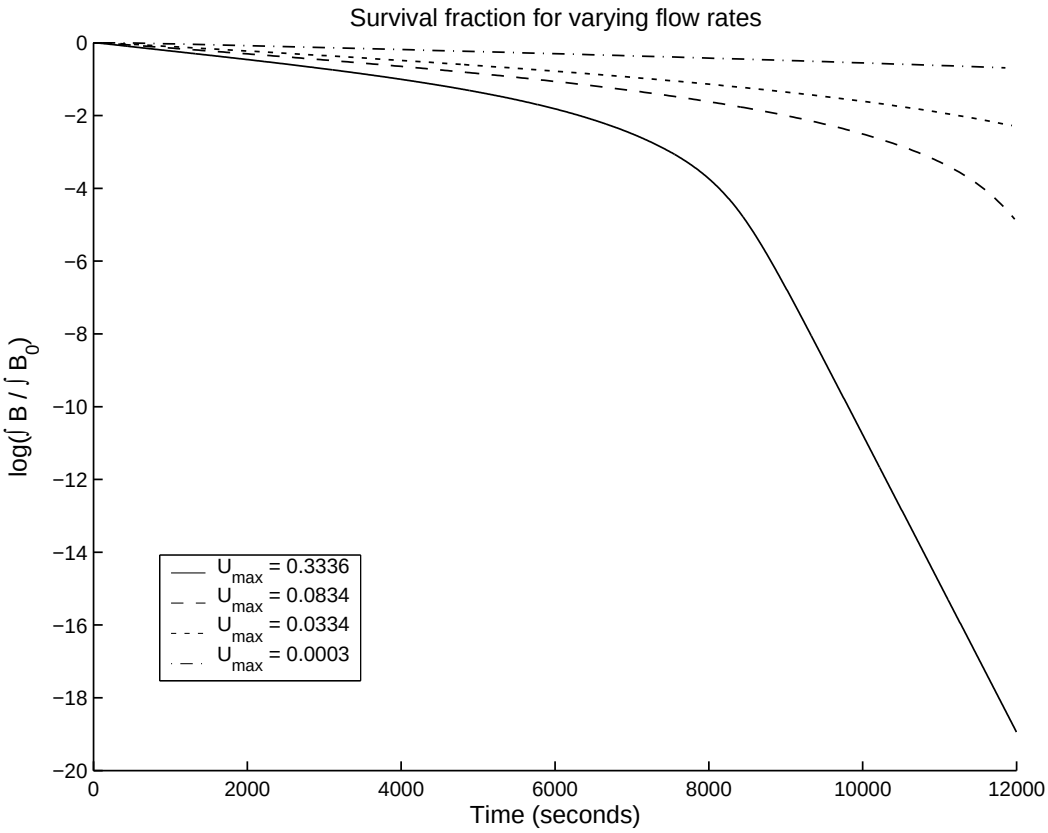

Figure 7: Survival curves for dosing at $C_s = 10\text{mgl}^{-1}$ and four flow rates (0.3336 m h^{-1}, 0.0834 m h^{-1}, 0.0334 m h^{-1} and 0.0033 m h^{-1}). Higher flow increases the susceptibility of the bacterial population resulting in earlier clearing of the bacteria.

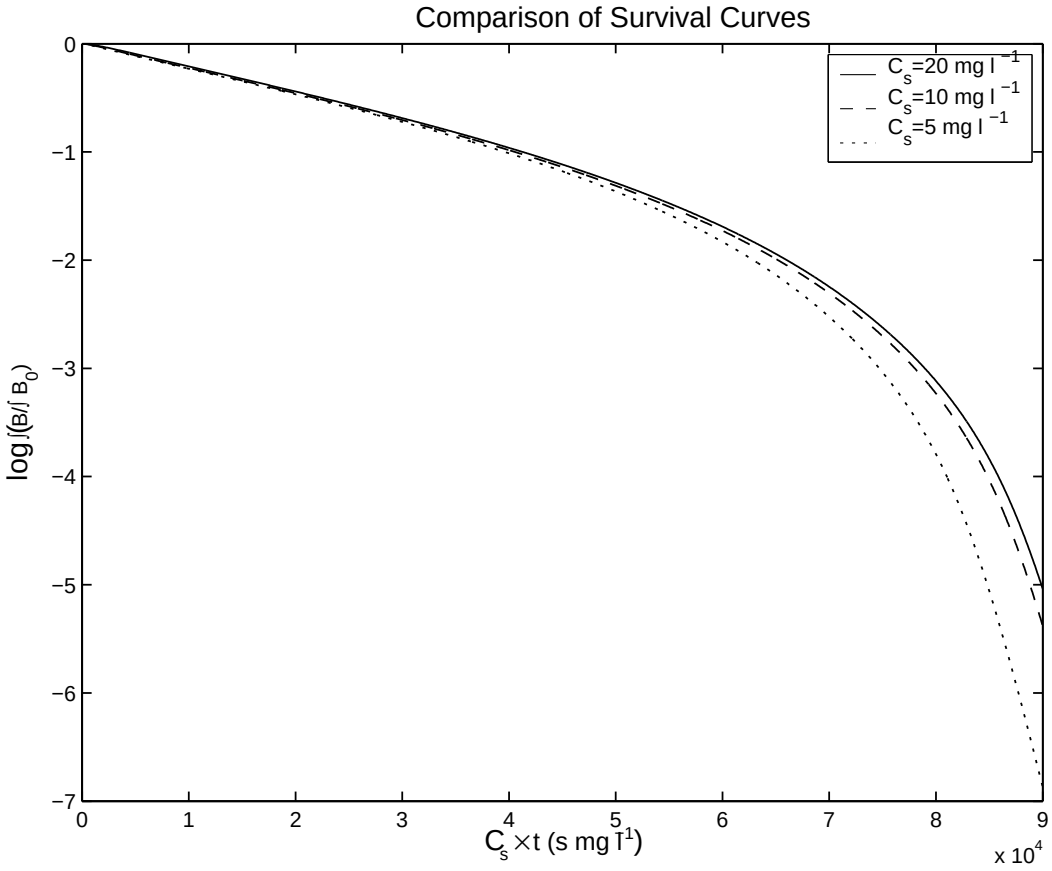

Figure 8: Survival curves for dosing at $C_s = 5\text{mgl}^{-1}$, $C_s = 10\text{mgl}^{-1}$ and $C_s = 20\text{mgl}^{-1}$. The horizontal axis is scaled by the product of the dose concentration and the dose length (chosen so that the product is constant) and the vertical axis is on a logarithmic scale. This comparison clearly illustrates that the dosing protocols do not give the same results. In fact, low concentration dosing for longer time is more effective.

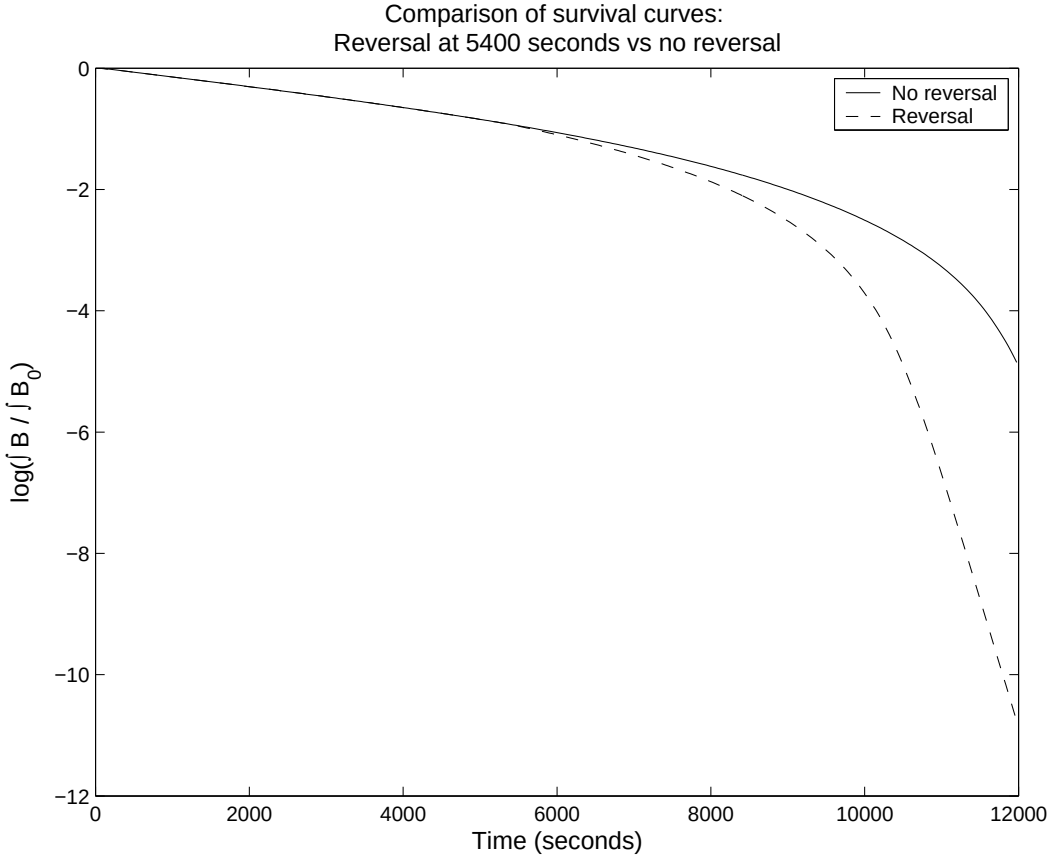

Figure 9: Comparison between two dosing protocols. The solid line shows resulting survival curve for continuous dosing, while the dashed line shows the survival curve when the flow is reversed at 5400 seconds. Because bacteria in regions upstream consume more nutrient, the bacteria in downstream regions are less susceptible to the antimicrobial agent. Reversing the flow exposes different bacteria to antimicrobial agent resulting in a more effective treatment.

ness of the treatment. Results from this simulation are shown in Figure 9. We see a dramatic decrease in the surviving population compared to the simulation without flow reversal. This indicates that manipulating the flow can increase the effectiveness of treatment.

3.8 Simulation 5: Continuous flow, non-reactive antimicrobial agent, variable surface roughness

We now examine the effect of surface roughness by comparing the survival curves for regions with three different fluid/biofilm interfaces. The biofilm/fluid interfaces, $\alpha(n)\Gamma(n)$ are given by

$$\Gamma(n) = \begin{cases} 0, & \text{for } x \leq 0.1 \\ (x-.1)(x+14.8) & \text{for } 0.1 < x \leq 0.2 \\ 1.5 + .2\sin\left(\frac{(x-0.2)}{.6} n\pi\right), & \text{for } 0.2 < x \leq 0.8 \\ (x-.9)(x-15.8) & \text{for } 0.8 < x \leq 0.9 \\ 0, & \text{for } 0.9 \leq x, \end{cases} \tag{15}$$

where the scalar parameter $\alpha(n)$ is chosen so that the areas of the biofilm regions are constant. Because the bacteria are uniformly distributed throughout the region, the total population of bacteria is constant for all n. We quantify 'roughness' by n (i.e. roughness increases with n).

The transport of nutrient and antimicrobial agent depends on the steady-state velocity profiles. Therefore the effectiveness of continuous dosing depends on the inflow velocity and the fluid/biofilm interface. To determine the effectiveness of treatment, several numerical simulations were done with varying interfaces and flow velocities. As n increases, we see a decrease in survival. In Figure 10, we show the steady-state flow streamlines, oxygen concentration profiles, interfaces and survival curves for $n = 0, 5$ and 11 for $U_{max} = 0.0334$ m h^{-1} and $U_{max} = 3.336$ m h^{-1}. (Note that the streamlines are the same for each flow rate since the fluid dynamics is governed by the Stokes equations.)

In Figure 11 we show the survival curves with low and high flow rates for the various biofilm regions. We find that for high flow velocities, such as this one, the survival curves are sensitive to the surface roughness. This is not the case for lower flow rates. There is very little difference between survival curves for the same values of n and $U_{max} = 0.0334$ m h^{-1}. Thus the interplay between the roughness and the flow leads to substantially different results.

In Figure 12, the survival curves for low and high flow rates are compared for each of the three regions tested. The general trend of lower survival for higher flow rates is consistent with the simulations in section 3.6.

4 Conclusions

We have presented a model of antimicrobial agent efficacy which couples fluid dynamics with the reaction, diffusion and advection of a single antimicrobial agent and nutrient. We use this model to investigate the mechanism of physiological resistance in two spatial dimensions. Our model reproduces results similar to those in [32], but also predicts spatial evolution of all chemicals and the bacterial population. The model makes no assumption about the mass transfer boundary layer or constituent concentration profiles. Because quantities in the model are spatially dependent, we are able to examine nutrient depleted zones in more detail. This motivated a simple dosing protocol which calls for flow reversal. This dosing strategy was shown to increase the effectiveness of dosing substantially. We also showed that long doses with low antimicrobial concentration is more effective in clearing bacteria than short doses of high antimicrobial concentration. Finally, we demonstrate that survival decreases with increasing fluid/biofilm interface roughness. This dependence is more pronounced at higher flow rates.

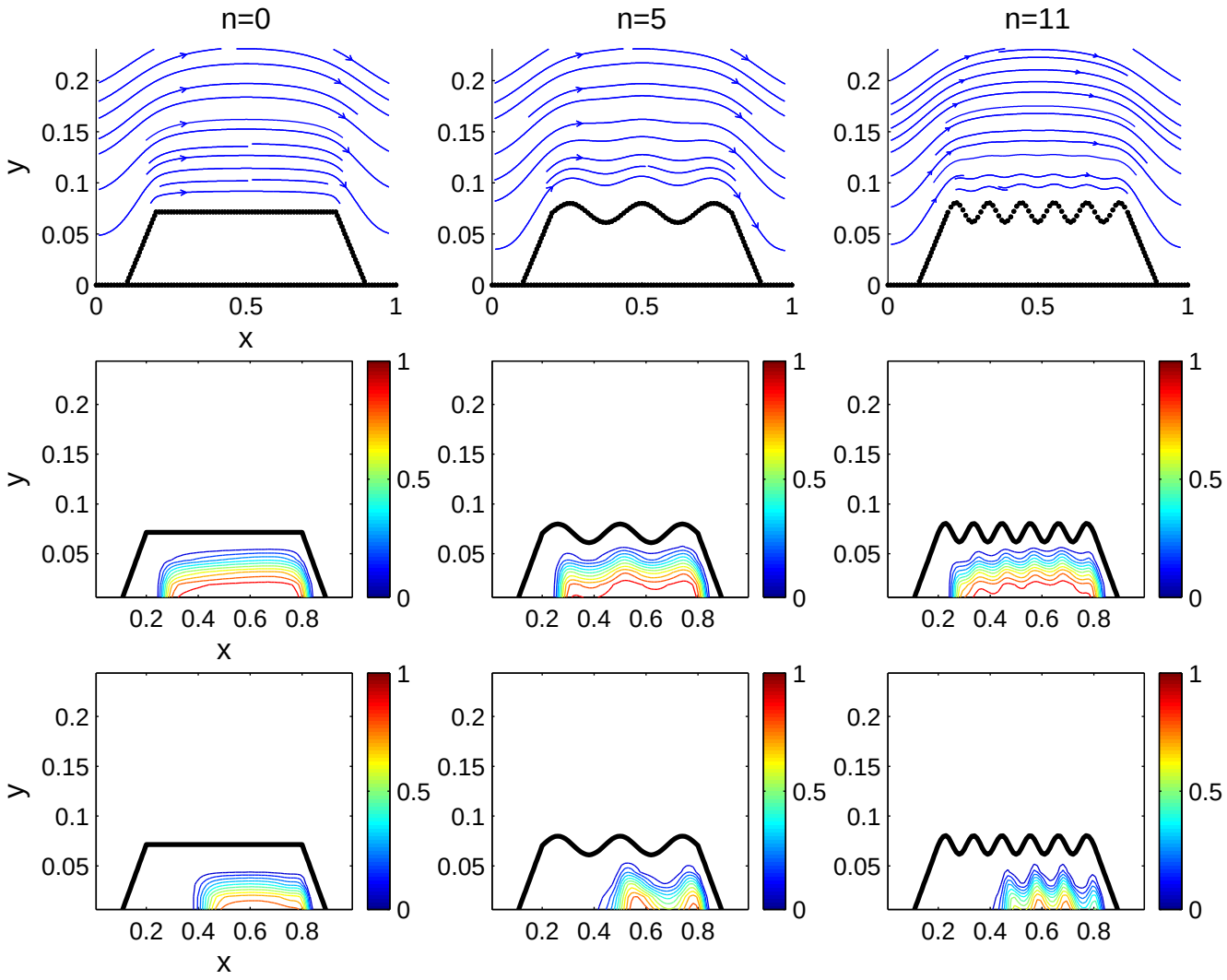

Figure 10: Top row: Streamlines for $n = 0, 5, 11$. Middle Row: Snapshots of the population of viable bacteria with low flow ($U_{max} = 0.0334$ m h^{-1}) at 7200 seconds. Bottom row: Snapshots of the population of viable bacteria with high flow ($U_{max} = 3.336$ m h^{-1}) at 7200 seconds. The roughness is quantified by the mode of the perturbation of the plateau region (see Equation (15)).

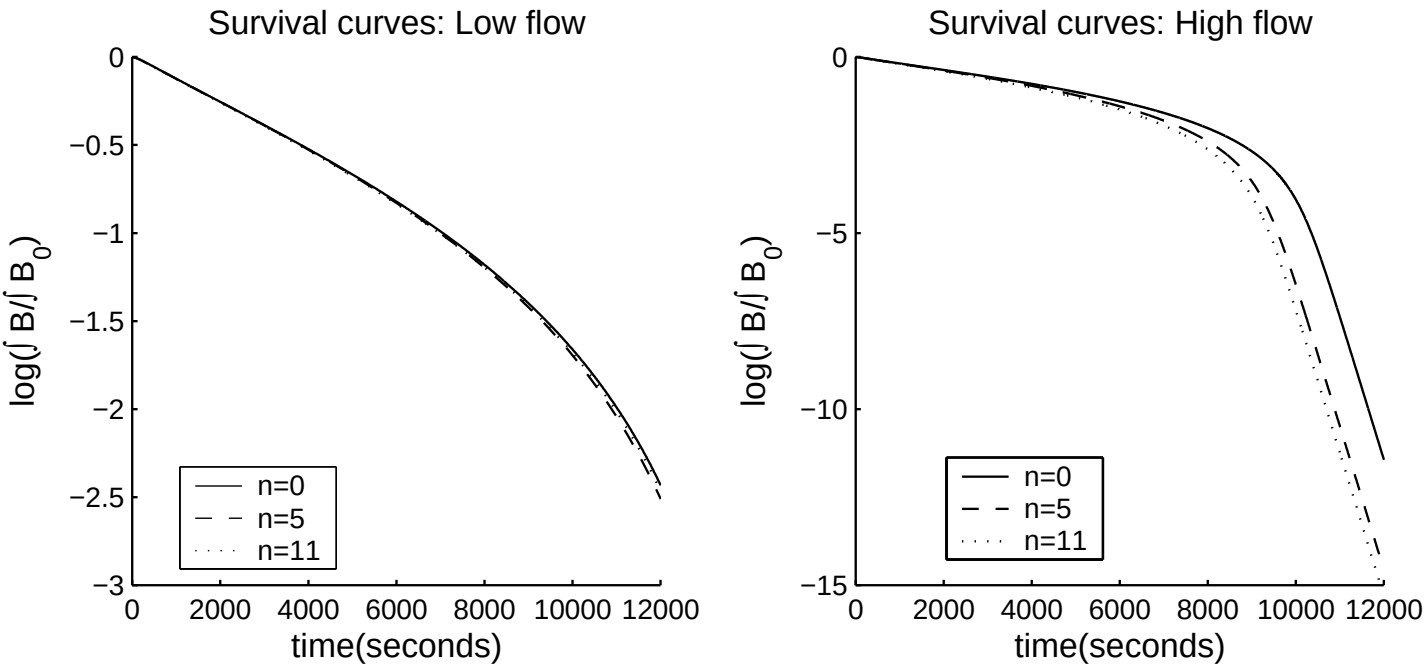

Figure 11: Survival curves for low flow ($U_{max} = .0334$m h^{-1}) and high flow ($U_{max} = 3.336$m h^{-1})showing that the difference in overall survival between the three modes, $n = 0, 5,$ and 11, is more pronounced for higher flow rates.

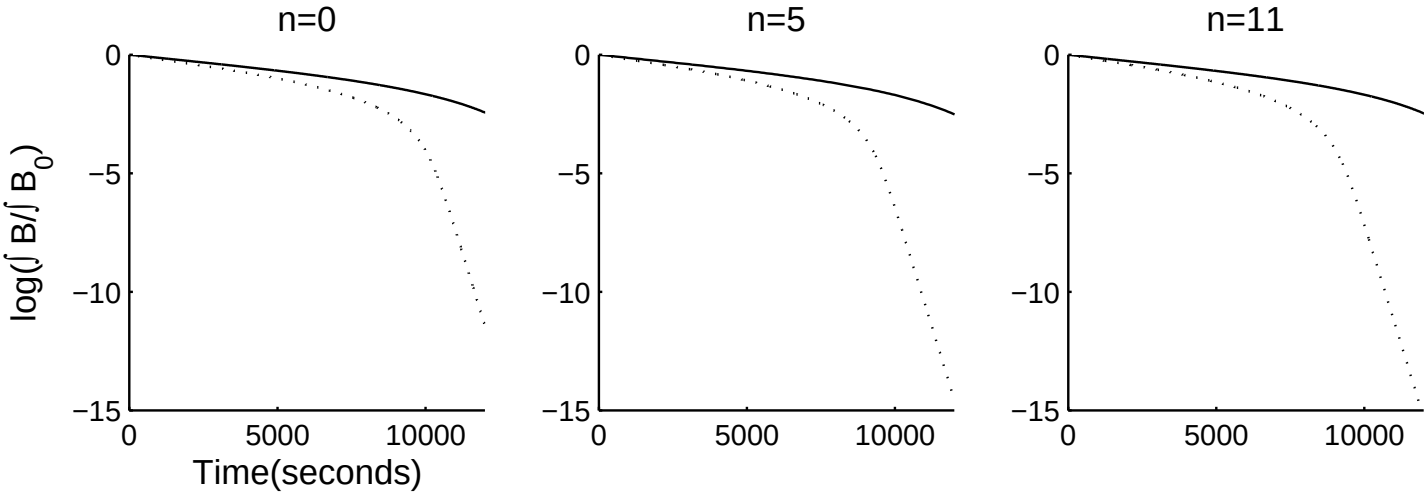

Figure 12: Survival curves for $n = 0, 5$ and 11 for flow rates of $U_{max} = 3.336$m h^{-1} (solid) and $U_{max} = .0334$m h^{-1} (dotted). Again we see that dosing at higher flow rates is more effective than lower flow rates.

We believe that the inclusion of comprehensive fluid mechanics, and the tracking of the spatial evolution of chemical constituents and bacterial population presents a robust and versatile method for studying dosing protocols in biofilm treatment. In the current study, we have not included changes in the geometry of the biofilm due to detachment, which is an important contributor to the dynamics of biofilm response to an antimicrobial agent. Within the current framework, we plan to model a dynamically evolving biofilm interface that responds both to fluid shear, detachment and bacterial growth. In this case, the Stokes equations of fluid dynamics must be solved at each time step due to the unsteady nature of the flow. We can incorporate evolution of the biofilm/fluid interface by using available information such as the mechanical stresses, as well as changes in material properties in response to antimicrobial application. In addition, this methodology will readily extend to a full three-dimensional implementation. The reaction-diffusion equations will be solved on a regular, finite difference grid. In 3D, the biofilm interface will be represented by discrete lattice points describing a surface, rather than discrete points that represent a one-dimensional curve. The grid-free method of regularized Stokeslets in 3D can easily handle forces distributed along such a surface [7].

A biological issue that has not been addressed in this manuscript is the existence of a small number of persister cells, which are not susceptible to treatment [21]. The nature of these persister cells is an open question. Current hypotheses include variation in multi-drug efflux pumps, maximum growth rates and deactivated programmed cell death (PCD) [21, 38, 17]. Although these hypotheses are not addressed in the current study, the current modeling framework will be used to investigate these theories.

4.1 Acknowledgments

This work was supported by the National Science Foundation Grant DMS-0201063. Computations were performed at the Center for Computational Science at Tulane and Xavier Universities, supported by the US Department of Energy contract DE-FG02-01ER63119.

The authors would also like to thank Dr. Philip Stewart for his help in this study.

References

[1] L. Adams and T. Charter, *New geometric immersed interface multigrid solvers*, SIAM Journal on Scientific Computing, 25 (2004), pp. 1516–1533.

[2] D. Allison and P. Gilbert, *Modification by surface association of antimicrobial susceptibility of bacterial populations*, Journal of Industrial Microbiology, 15 (1995), pp. 311–317.

[3] H. Beyenal and Z. Lewandowski, *Mass-transport dynamics, activity and structure of sulfate-reducing biofilms*, AIChE Journal, 47 (2001), pp. 1689–1697.

[4] W. G. Characklis and K. C. Marshall, eds., *Biofilms*, John Wiley and Sons, inc., 1990.

[5] C.-I. Chen, M. Reinsel, and R. Mueller, *Kinetic investigation of microbial souring in porous media using microbial consortia from oil reservoirs*, Biotechnology and Bioengineering, 44 (1994), pp. 263–269.

[6] R. Cortez, *The method of regularized stokeslets*, SIAM Journal of Scientific Computing, 23 (2001), pp. 1204–1224.

[7] R. Cortez, L. Fauci, and A. Medovikov, *The method of regularized stokeslets in three dimensions: Analysis, validation, and application to helical swimming*, Physics of Fluids, (2004).

[8] J. Costerton, P. S. Stewart, and E. P. Greenberg, *Bacterial biofilms: A common cause of persistent infections*, Science, 284 (1999), pp. 1318–1322.

[9] D. Davies, *Understanding biofilm resistance to antibacterial agents*, Nature Reviews Drug Discovery, 2 (2003), pp. 114–122.

[10] D. DeBeer, P. Stoodley, and z. Lewandowski, *Liquid flow and mass transfer in heterogeneous biofilms*, Water Research, 30 (1996), pp. 2761–2765.

[11] J. Dockery and I. Klapper, *Finger formation in biofilm layers*, SIAM Journal on Applied Mathematics, 62 (2002), pp. 853–869.

[12] M. G. Dodds, K. J. Grobe, and P. S. Stewart, *Modeling biofilm antimicrobial resistance*, Biotechnology and Bioengineering, 68 (2000), pp. 456–465.

[13] H. Eberl, C. Picioreanu, J. Heijnen, and M. van Loosdrecht, *A three-dimensional numerical study on the correlation of spatial structure, hydrodynamic conditions , and mass transfer and conversion in biofilms*, Chemical Engineering Science, 55 (2000), pp. 6209–6222.

[14] J. G. Elkins, D. J. Hassett, P. S. Stewart, H. P. Schweizer, and T. R. McDermott, *Protective role of catalase in Pseudomonas aeruginosa biofilm resistance to hydrogen peroxide*, Applied and Environmental Microbiology, 65 (1999), pp. 4594–4600.

[15] G. H. Golub and C. F. V. Loan, *Matrix Computations*, Johns Hopkins University Press, 3 ed., 1996.

[16] K. Grobe, J. Zahler, and P. Stewart, *Role of dose concentration in biocide efficacy against Pseudomonas aeruginosa biofilms*, Journal of Industrial Microbiology and Biotechnology, 29 (2002), pp. 10–15.

[17] M. Hentzer, H. Wu, J. B. Andersen, K. Riedel, T. B. Rasmussen, N. Bagge, N. Kumar, M. A. S. nd Zhijun Song, P. Kristoffersen, M. Manefield, J. W. Costerton, S. Molin, L. Eberl, P. Steinberg, S. Kjelleberg, N. Hoiby, and M. Givskov, *Attenuation of Pseudomonas aeruginosa virulence by quorum sensing inhibitors*, The EMBO Journal, 22 (2003), pp. 3803–3815.

[18] I. Klapper, C. Rupp, R. Cargo, B. Purvedorj, and P. Stoodley, *Viscoelastic fluid description of bacterial biofilm material properties*, Biotechnology and Bioengineering, 80 (2002), pp. 289–296.

[19] H. M. Lappin-Scott and J. W. Costerton, eds., *Microbial Biofilms*, Cambridge University Press, Cambridge, 1995, ch. Mechanisms of the Protection of Bacterial Biofilms from Antimicrobial Agents, pp. 118–130.

[20] R. J. Leveque and Z. Li, *The immersed interface method for elliptic equations with discontinuous coefficients and singular sources*, SIAM Journal of Numerical Analysis, 31 (1994), pp. 1019–1044.

[21] K. Lewis, *Riddle of biofilm resistance*, Antimicrobial Agents and Chemotherapy, 45 (2001), pp. 999–1007.

[22] J. M. Lighthill, *An informal introduction to theoretical fluid mechanics*, Oxford University Press, New York, 1986.

[23] J. Manem and B. Rittmann, *Removing trace level organic pollutants in a biological filter.*, Journal of American Water Works, 84 (1992), pp. 152–157.

[24] E. Morgenroth, H. Eberl, and M. van Loosdrecht, *Evaluating 3-d and 1-d mathematical models for mass transport in heterogeneous biofilms*, Water Science and Technology, 41 (2000), pp. 347–356.

[25] C. Nicolella, M. van Loosdrecht, and J. Heijnen, *Mass transfer and reaction in a biofilm airlift suspension reactor*, Chemical Engineering Science, 53 (1998), pp. 2743–2753.

[26] D. Noguera, S. Okabe, and C. Picioreanu, *Biofilm modeling: Present status and future directions*, Wat. Sci. Tech, 39 (1999), pp. 273–278.

[27] C. Picioreanu, M. van Loosdrecht, and J. Heijnen, *A theoretical study on the effect of surface roughness on mass transport and transformation in biofilms*, Biotechnology and Bioengineering, 68 (2000), pp. 355–269.

[28] C. Picioreanu, M. C. van Loosdrecht, and J. J. Heijnan, *Two-dimensional model of biofilm detachment caused by internal stress from liquid flow*, Biotechnology and Bioengineering, 72 (2001), pp. 205–218.

[29] C. Potera, *Forging a link between biofilms and disease*, Science, 283 (1999), pp. 1837–1839.

[30] C. Pozrikidis, *Numerical computation in science and engineering*, Oxford University Press, New York, 1998.

[31] B. Prakash, B. Veeregowda, and G. Krishnappa, *Biofilms: A survival strategy of bacteria*, Current Science India, 85 (2003), pp. 1299–1307.

[32] M. E. Roberts and P. S. Stewart, *Modeling antibiotic tolerance in biofilms by accounting for nutrient limitation*, Antimicrobial Agents and Chemotherapy, 48 (2004), pp. 48–52.

[33] S. S. Sanderson and P. S. Stewart, *Evidence of bacterial adaption to monochloramine in Pseudomonas aeruginosa biofilms and evaluation of biocide action model*, Biotechnology and Bioengineering, 56 (1997), pp. 201 – 209.

[34] P. S. Stewart, *Diffusion in biofilms*, Journal of Bacteriology, 185 (2003), pp. 1485–1491.

[35] P. S. Stewart, F. Roe, J. Rayner, J. G. Elkins, Z. Lewandowski, U. A. Ochsner, and D. J. Hassett, *Effect of catalase on hydrogen peroxide penetration into Pseudomonas aeruginosa biofilms*, Applied and Environmental Microbiology, 66 (2000), pp. 836–838.

[36] P. Stoodley, D. deBeer, J. Boyle, and H. L.-S. t, *Evolving perspectives of biofilm structure*, Biofouling, (1999).

[37] P. Stoodley, A. Jacobsen, B. Dunsmore, B. Purevdorj, S. Wilson, H. Lappin-Scott, and J. Costerton, *The influence of fluid shear and $alcl_3$ on the material properties of Pseudomonas aeruginosa pao1 and Desulfovibrio sp. ex265 biofilms*, Water Science and Technology, 43 (2001), pp. 113–120.

[38] N. Sufya, D. Allison, and P. Gilbert, *Clonal variation in maximum specific growth rate and susceptibility towards antimicrobials*, Journal of Applied Microbiology, 95 (2003), pp. 1261–1267.

[39] O. Wanner and P. Reichert, *Mathematical modeling of mixed-culture biofilms*, Biotechnology and Bioengineering, 49 (1996), pp. 172–184.

[40] J. Wingender, T. R. Neu, and H.-C. Fleming, *Microbial Extracellular Polymeric Substances. Characterization, Structure and Function*, Springer Verlag, 1999.

[41] J. Yu, M. Ji, and P. Yue, *A three-phase fluidized bed reactor in the combined anaerobic/aerobic treatment of wastewater*, Journal of Chemical Technology and Biotechnology, 74 (1999), pp. 619–626.

[42] X. Zhang and P. L. Bishop, *Spatial distribution of extracellular polymeric substances in biofilms*, Journal of Environmental Engineering, 127 (2001), pp. 850 – 856.